

Crystal growth and metallic ferromagnetism induced by electron doping in FeSb₂

Mohamed A. Kassem^{1,2}, Yoshikazu Tabata¹, Takeshi Waki¹, Hiroyuki Nakamura¹

¹ Department of Materials Science and Engineering, Kyoto University, Kyoto 606-8501, Japan,

² Department of Physics, Faculty of Science, Assiut University, Assiut 71516, Egypt,

Abstract:

In order to study the metallic ferromagnetism induced by electron doping in the narrow-gap semiconductor FeSb₂, single crystals of FeSb₂, Fe_{1-x}Co_xSb₂ ($0 \leq x \leq 0.5$) and FeSb_{2-y}Te_y ($0 \leq y \leq 0.4$), were grown by a simplified self-flux method. From powder x-ray diffraction (XRD) patterns, wavelength-dispersive x-ray spectroscopy (WDX) and x-ray Laue diffraction, pure and doped high-quality single crystals, within the selected solubility range, show only the orthorhombic *Pnmm* structure of FeSb₂ with a monotonic change in lattice parameters with increasing the doping level. In consistence with the model of nearly ferromagnetic small-gap semiconductor, the energy gap of FeSb₂ Pauli paramagnet gradually collapses by electron doping before it closes at about x or $y \approx 0.15$ and subsequent itinerant electron anisotropic ferromagnetic states are observed with higher doping levels. A magnetic phase diagram is established and discussed in view of proposed theoretical scenarios.

Keywords: Single crystals; narrow-gap semiconductor; Kondo insulator; itinerant-electron ferromagnetism.

1. Introduction

Intermetallic compounds are usually metallic. However, some compounds including the rare-earth based typical Kondo insulators such as SmB_6 and YbB_{12} intermetallics and the proposed transition-metal counterparts FeSi and FeSb_2 show a semiconductor behavior and are described as strongly correlated semiconductors¹⁻⁴. In these compounds, generally, itinerant and localized electrons hybridize and open a narrow gap at the Fermi level with a large density of states⁵. As many iron- and ruthenium-based semiconductors, FeSb_2 has attracted a considerable attention because of its unusual transport and magnetic behavior as well as its notable thermoelectric properties^{4,6,7}. FeSb_2 and FeSi were suggested as examples of non-rare-earth based Kondo semiconductors⁸. Moreover, according to the recent theoretical study, FeSb_2 is proposed as a nearly ferromagnetic small gap semiconductor and one can switch from a small gap semiconductor to a ferromagnetic metal with magnetic moment $\approx 1\mu_B$ per Fe ion by external magnetic field⁹.

Common nonmagnetic insulating state with thermal activation-type magnetization process have been observed for poly- and single-crystalline samples of FeSb_2 . However, some previously presented physical properties of FeSb_2 depend on the sample and has been elucidated as very sensitive to ppm-level impurities. For example, anisotropic insulating behavior with a metal-insulator transition at 50 K along the b -axis observed by Petrovic *et al.* contrasts the almost isotropic insulating behavior down to 10 K along the three principal axes observed by other groups^{4,7,10}. Further, a reported colossal Seebeck coefficient of -45 mV K^{-1} at 10 K observed by Bientien *et al.* has not been observed in single crystals prepared by others^{6,11}. The questionable reproducibility in the large Seebeck effect has recently attributed to a phonon-drag effect⁷.

The magnetization M of FeSi (cubic B20 structure) and FeSb_2 (orthorhombic marcasite structure) shows an activation-type increase with increasing temperature T above 70 and 50 K, respectively^{12,13}. After showing a broad maximum around 500 and 300 K, respectively, the M - T curve exhibits a Curie-Weiss like behavior^{12,13}. In order to explain the magnetization process of FeSi , a model was proposed in Takahashi's spin fluctuation theory that employed a simple density of states curve with an energy gap E_g and considered quantum spin fluctuations together with thermal spin fluctuations^{14,15}. The model has succeeded to evaluate E_g (~ 62 and 30 meV for FeSi and FeSb_2 , respectively) from the experimental magnetization data and to predict its pressure-dependence in qualitative consistence with results of resistivity measurements¹⁶⁻¹⁸.

On the other hand, the Kondo description of FeSb_2 suggests that the substitution of third element can give rise to drastic changes in the electronic and magnetic states¹⁹. Emergence of ferromagnetic and antiferromagnetic states have been observed by substitutions with Co and Cr for Fe and by Te for Sb²⁰⁻²². However, as well as the properties of FeSb_2 , the reproducibility of its solid solutions properties needs investigation^{4,20-22}. Further, the study of the energy gap evolution by doping, estimated from magnetization based on the itinerant-electron magnetism scenario proposed in Takahashi's spin fluctuation theory, would imply how much the model fits to explain the experimental results and hence the origin of magnetization process in this system.

Here, we report simple self-flux crystal growth of high-quality FeSb_2 and its electron-doped solid solutions, $\text{Fe}_{1-x}\text{Co}_x\text{Sb}_2$ ($0 \leq x \leq 0.5$) and $\text{FeSb}_{2-y}\text{Te}_y$ ($0 \leq y \leq 0.4$). The evolution of the

energy gap to metallic ferromagnetic states by electron doping is studied from a viewpoint of Takahashi's theory of itinerant electron magnetism. A magnetic phase diagram of electron doped FeSb₂ is presented.

2. Materials and Methods

Large single crystals of FeSb₂, Fe_{1-x}Co_xSb₂ ($0 \leq x \leq 0.5$) and FeSb_{2-y}Te_y ($0 \leq y \leq 0.4$) were synthesized by a high temperature Sb self-flux method. Lumps of Fe (99.95 % Alfa Aesar) and Co (99.9 % Kojundo Chemical Laboratory Co., Ltd.) and grains of Sb (99.999 % Kojundo Chemical Laboratory Co., Ltd.) and Te (99.999 % Kojundo Chemical Laboratory Co., Ltd.) have been used. A mixture of Fe: Sb, (Fe_{1-x}Co_x): Sb or Fe: (Sb_{2-y}Te_y) with a molar ratio equal to 8: 92 has been sealed without crucibles in an evacuated quartz tube (1 cm in diameter) with a dimple. The ampule was heated in a muffle furnace and kept at 1000°C for 2 hours then cooled down to 800°C over 10 hours and finally slowly cooled down to 650°C over 100 hours. The ampule has been taken out from the furnace at 650°C and subsequently turned upside down to separate the flux liquid from grown crystals. The excess flux attached to the surface of picked-up crystals has been removed by a further sealing in a long quartz ampule heated for 24 hours in a temperature-gradient horizontal furnace with the sample at the highest temperature of 800°C.

Crushed powder of a part of the grown crystals were investigated at room temperature by powder XRD (PANalytical, X'Pert Pro) with Cu $K_{\alpha 1}$ radiation monochromated by a Ge (111)-Johansson-type monochromator. The crystal structure parameters were refined by the Rietveld refinement analysis using TOPAS (Bruker) software. The actual chemical compositions were investigated by SEM-WDX (Hitachi, S-3500H). The crystallinity level and crystalline axes were determined by the x-ray Laue method.

Magnetization and magnetic anisotropy were measured in a temperature range of $T = 2 - 350$ K using a SQUID magnetometer (Quantum Design, MPMS-7) installed in the LTM center of Kyoto University. Three single crystals of FeSb₂ were cut and polished in rectangular rod shapes along the different principal crystal-axes for electrical resistivity, $\rho(T)$, measurements. $\rho(T)$ was measured at zero magnetic field in a temperature range of $T = 4 - 300$ K by employing the four-probe method.

3. Results and discussion

Grown single crystals with the long axis parallel to the b axis and others with large $\{110\}$ faces (as shown in the inset of Fig. 1(a)) are large enough for different macroscopic investigations. The synthesized phase and crystal structure of the grown crystals were investigated by powder XRD for crushed parts. The observed XRD patterns shown in Fig. 1(a) are fitted by the Rietveld method using the structure parameters of FeSb₂ marcasite structure of $Pnmm$ orthorhombic symmetry. No extra phases, other than the FeSb₂ phase, in the pristine and solid solutions within the selected solubility range were observed. In consistence with Vegard's law, lattice parameters as well as the unit cell volume show monotonic variations with the doping levels x and y indicating successful substitution of Co for Fe and Te for Sb in the single-phase solid solutions. WDX reveals actual chemical compositions very close to the starting compositions of FeSb₂, Fe_{1-x}Co_xSb₂ and FeSb_{2-y}Te_y. The grown single crystals are of high

quality as seen in the shiny surface and clearly indicated in its Laue patterns as presented in Fig. 1(b) showing the bulk-structure symmetry for a (110) plane.

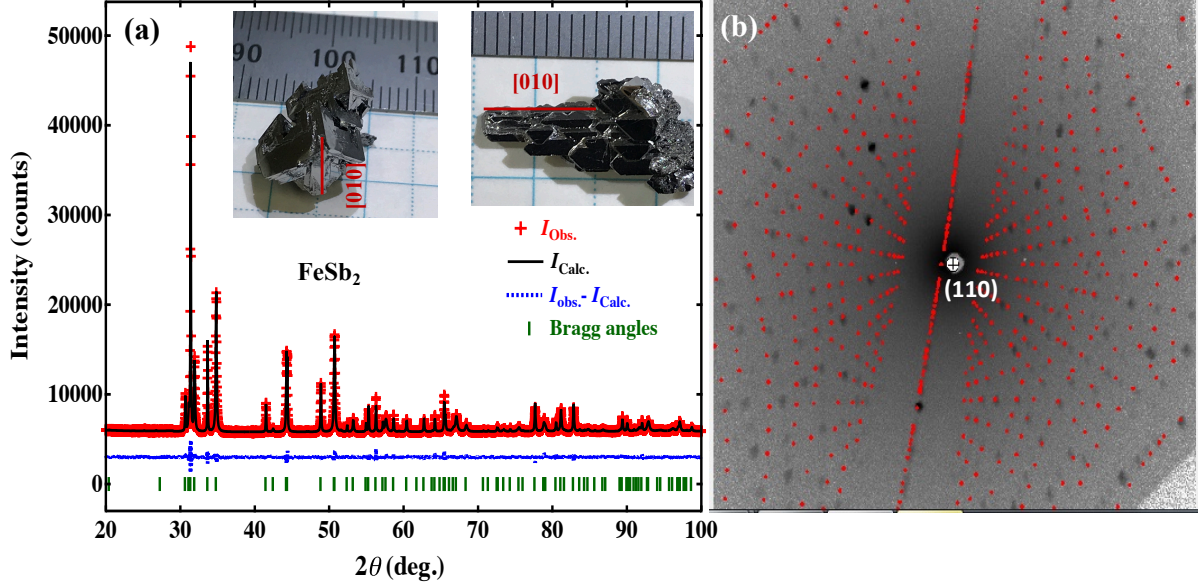


Figure 1: (a) The XRD pattern of powder crushed from the grown crystals of FeSb₂ shown with a calculated pattern by the Rietveld refinement. Insets are photos of typical crystals. (b) Observed and calculated Laue pattern of a (110) plane.

Figure 2(a) shows the temperature dependence of electrical resistivity, $\rho(T)$, of FeSb₂ measured with applying current along the three principal crystal axes. We have not observed the large anisotropy with the metal-insulator transition at 50 K along the b -axis reported by Petrovic et al.⁴, instead and as recently reported⁷, an almost isotropic semiconducting behavior down to 4 K, indicating two intrinsic energy gaps, was observed. We have estimated about 2.5 and 33 meV for the two intrinsic energy from the data below 300 K¹⁰, which are in consistence with reported values^{6,8}. The Arrhenius plot to estimate the main energy gap (E_g) from the linear fit in the temperature range $T = 70 - 130$ K is shown in the inset of Fig. 2(a).

Figure 2(b) shows the temperature dependences of the magnetic susceptibility, χ , of FeSb₂ measured under applied fields H parallel to the three principal crystal axes, χ_a , χ_b and χ_c . Similar results are reported for high quality crystals, namely anisotropic χ with almost identical behavior in a and b directions and diamagnetic to paramagnetic crossover only for $H // c$, at $T \simeq 70$ K. Small upturns at low T are attributed to possible tiny amounts of magnetic impurities. The unusual magnetic properties of FeSb₂ of a thermal activation type above about 50 K are similar to those of FeSi^{4,13}, recently discussed by using a simple semiconductor-model based on the Takahashi's theory^{18,23}. As itinerant electrons in conduction bands behave like non-interacted moments due to the effect of spin fluctuations, χ of FeSb₂ can be assumed to come mainly from thermally excited electrons in the conduction bands and holes in the valance bands, separated by an energy gap E_g . The susceptibility of each electron (hole), χ_e (χ_h), is proportional to $1/T$ and the number of the excited electrons (holes), n_e (n_h), is proportional to

$T^{3/2}\exp(-E_g/2k_B T)$, where k_B is the Boltzmann constant. Hence, the total susceptibility $\chi(T) = 2n_e(T)\chi_e(T)$ is given as,

$$\chi(T) = AT^{1/2}e^{-E_g/2k_B T}. \quad (1)$$

Linear fitting of $\ln(\chi_{\text{avg}}T^{1/2})$ vs. $1/T$ in the temperature range $140 \text{ K} < T < 220 \text{ K}$ shown as the inset in Fig. 2(b), where $\chi_{\text{avg}} = (\chi_a + \chi_b + \chi_c)/3$ is the polycrystalline averaged susceptibility, yields $E_g = 428.08 \pm 13 \text{ K}$ ($36.89 \pm 1.12 \text{ eV}$). The value is in consistency with value estimated above from $\rho(T)$ (33 meV) and agrees with reported results from both magnetization and resistivity measurements^{6,10,17,18}. The observed magnetic and electronic transport properties indicate the high quality of our FeSb₂ single crystals.

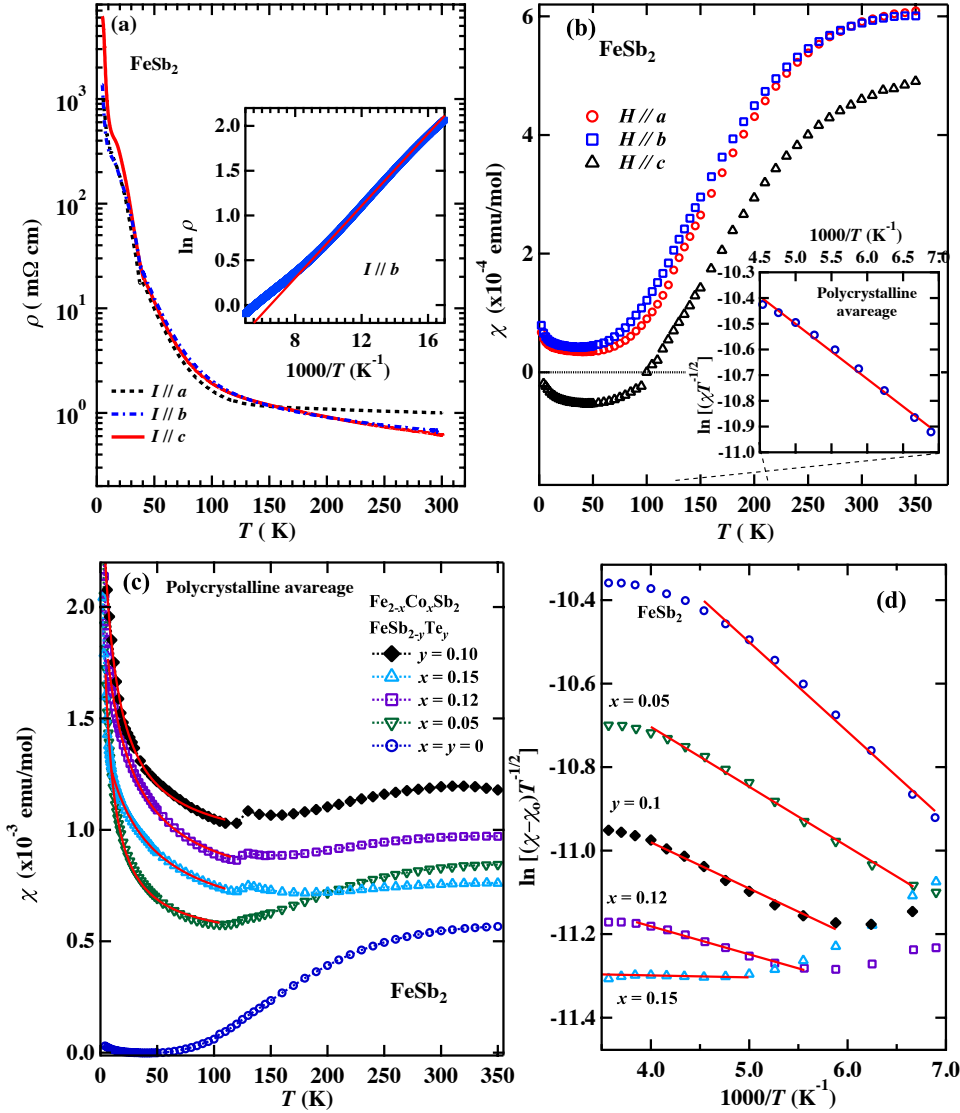


Figure 2: (a) The electrical resistivity $\rho(T)$ of FeSb₂ measured with currents applied along three principal crystal axes. Inset shows the Arrhenius plot of $\rho_b(T)$. The solid line represents a linear fit of the data. (b) Magnetic susceptibility $\chi(T)$ of FeSb₂ measured at $H = 0.1$ T applied along principal crystal axes. Inset shows the plot of $\ln(\chi_{\text{avg}}T^{1/2})$ vs. $1/T$ and its linear fit in a solid line. (c) $\chi(T)$ data of Fe_{1-x}Co_xSb₂ and FeSb_{2-y}Te_y at low doping levels. Solid lines are fits to a modified Curies-Weiss law at temperatures below 115 K. (d) $\ln(\chi_{\text{avg}}T^{1/2} - \chi_0)$ vs. $1/T$ plots and their linear fits (solid lines) for Fe_{1-x}Co_xSb₂ and FeSb_{2-y}Te_y with x and y up to 0.15.

Electron doping to FeSb₂ influences its energy gap and results in a gradual evolution to metallic ferromagnetic state^{20,22}. **Figure 2(c)** shows the temperature dependences of susceptibility, $\chi(T)$, of Fe_{1-x}Co_xSb₂ and FeSb_{2-y}Te_y at low doping levels below x and $y = 0.15$. The thermal activation of $\chi(T)$ gradually decreases with doping and competing paramagnetic upturns emerge below about 100 K. Anomalies observed around 130 K may be attributed to a possible magnetic transition due to this competition between the base Pauli paramagnetic and emerging magnetic states. To investigate the evolution of the energy gap by doping, from data above 140 K as in the case of FeSb₂, one has to consider a temperature-independent contribution, χ_0 , coming from the low-temperature emergent paramagnetic state. We modify equation (1) to estimate the $\chi(T)$ after low-level doping that becomes,

$$\chi(T) = \chi_0 + AT^{1/2}e^{-E_g/2k_B T} \quad (2)$$

The temperature-independent term χ_0 also contributes in the low-temperature paramagnetic state. The susceptibility behavior below about 120 K can be described by a modified Curie-Weiss (CW) law, $\chi(T) = \chi_0 + \frac{C}{T - \theta_W}$, where C is the Curie constant and θ_W is the Weiss temperature. We have estimated the value of χ_0 at different doping levels by fitting data below about 115 K to the modified CW law. Fittings are shown by solid lines in **Fig. 2(c)**. **Figure 2(d)** shows the $\ln[(\chi_{\text{avg}} - \chi_0)T^{1/2}]$ vs. $1/T$ plots for Fe_{1-x}Co_xSb₂ and FeSb_{2-y}Te_y of x and y up to 0.15 for the high temperature data within 150 - 250 K using χ_0 estimated from data below 115 K as described above. Linear fits result in a gradual decrease in the energy gap that closes at about $x = 0.15$. Estimated values of χ_0 and E_g are presented in **table 1**.

Further electron doping to the nonmagnetic narrow-gap semiconductor results in an induced weakly itinerant electron ferromagnetism in FeSb₂^{20,22}. **Figure 3** shows the magnetic susceptibility, $M(T)/H$, and its anisotropy in Fe_{1-x}Co_xSb₂ and FeSb_{2-y}Te_y with x up to 0.5 and y up to 0.4 measured at a field $H = 0.1$ T. As previously observed²⁰, with substituting Co for Fe ($3d$ -electron doping), weak ferromagnetic states below $T_C \simeq 7$ K with the highest magnetic moment of $0.0011 \mu_B/d$ -element are observed, **Fig. 3(c)**. However, different anisotropic behavior is observed here. The FM state emerges first in the b direction at about $x \simeq 0.2$ while in the other two directions emerges at $x = 0.3$ and again disappears in the a and c directions for higher doping levels. Further, our observation of a FM state emerges in the c direction at $x = 0.3$ varies from previously reported results²⁰. We attribute these differences to a sample dependence of magnetization anisotropy similar to the resistivity.

The $5p$ -electron doping by substituting Te for Sb results in significantly stronger ferromagnetic states than the d -electron doping²². **Figure 3(d)** show the temperature dependence of $M(T)/H$ of FeSb_{2-y}Te_y with y up to 0.4 at a field $H = 0.1$ T applied along the b -axis. Anisotropic magnetic behavior is shown in **Fig. 3(e)** for $y = 0.4$ with b is the easy axis, being deferent from the a easy axis in Fe_{1-x}Co_xSb₂. Gradual increases of both M up to $0.015 \mu_B/\text{Fe}$, see **Fig. 3(f)**, and T_C up to 85 K are observed in contrast to the result of d -electron doping, with two orders of magnitude higher in both M and T_C for y and $x \simeq 0.4$. The inset of **Fig. 3(d)** shows the temperature dependences of inverse susceptibility for selected Fe_{1-x}Co_xSb₂ and FeSb_{2-y}Te_y which clarify the gradual change in the susceptibility from the thermal activated type to the CW behavior. Dashed lines are the fit to a modified CW law. Another difference is the Weiss temperature, $\theta_W \simeq -70$ K, for $y = 0.4$, compared to $\theta_W \simeq 3$ K for $x = 0.3$, which implies the coexistence of

an antiferromagnetic (AF) component in $\text{FeSb}_{2-y}\text{Te}_y$. A canted AF state has been reported in this system by Hu et al²². Magnetic parameters of both systems, $\text{Fe}_{1-x}\text{Co}_x\text{Sb}_2$ and $\text{FeSb}_{2-y}\text{Te}_y$, are presented in table 1. The observed values of μ_{eff}/μ_s much higher than standard value of the localized system, $\mu_{\text{eff}}/\mu_s \sim 1$, indicate the itinerant-electron FM nature of the studied systems.

Figure 4 shows the magnetic phase diagram of $\text{Fe}_{1-x}\text{Co}_x\text{Sb}_2$ and $\text{FeSb}_{2-y}\text{Te}_y$ ($0 < x$ and $y < 0.6$) showing the evolution of the energy gap E_g , closed circles for $\text{Fe}_{1-x}\text{Co}_x\text{Sb}_2$ and closed square for $\text{FeSb}_{2-y}\text{Te}_y$, estimated from M data. The value of E_g for FeSb_2 is in consistence with that estimated from resistivity, open diamond from our results above and open square and triangle by Bentein et al. and Takahashi et al. respectively^{6,8}. The energy gap collapses by the electron doping and closes completely at $x, y \approx 0.15$ before the emergence of a FM metallic state that becomes strongest at around $x, y \approx 0.5$. Suppression of the FM state towards the nonmagnetic compounds, CoSb_2 and FeTe_2 , has been observed above $x = y \approx 0.5$ ^{20,22}. The inset shows the composition dependence of T_C of $\text{Fe}_{1-x}\text{Co}_x\text{Sb}_2$ and $\text{FeSb}_{2-y}\text{Te}_y$. The observed monotonic

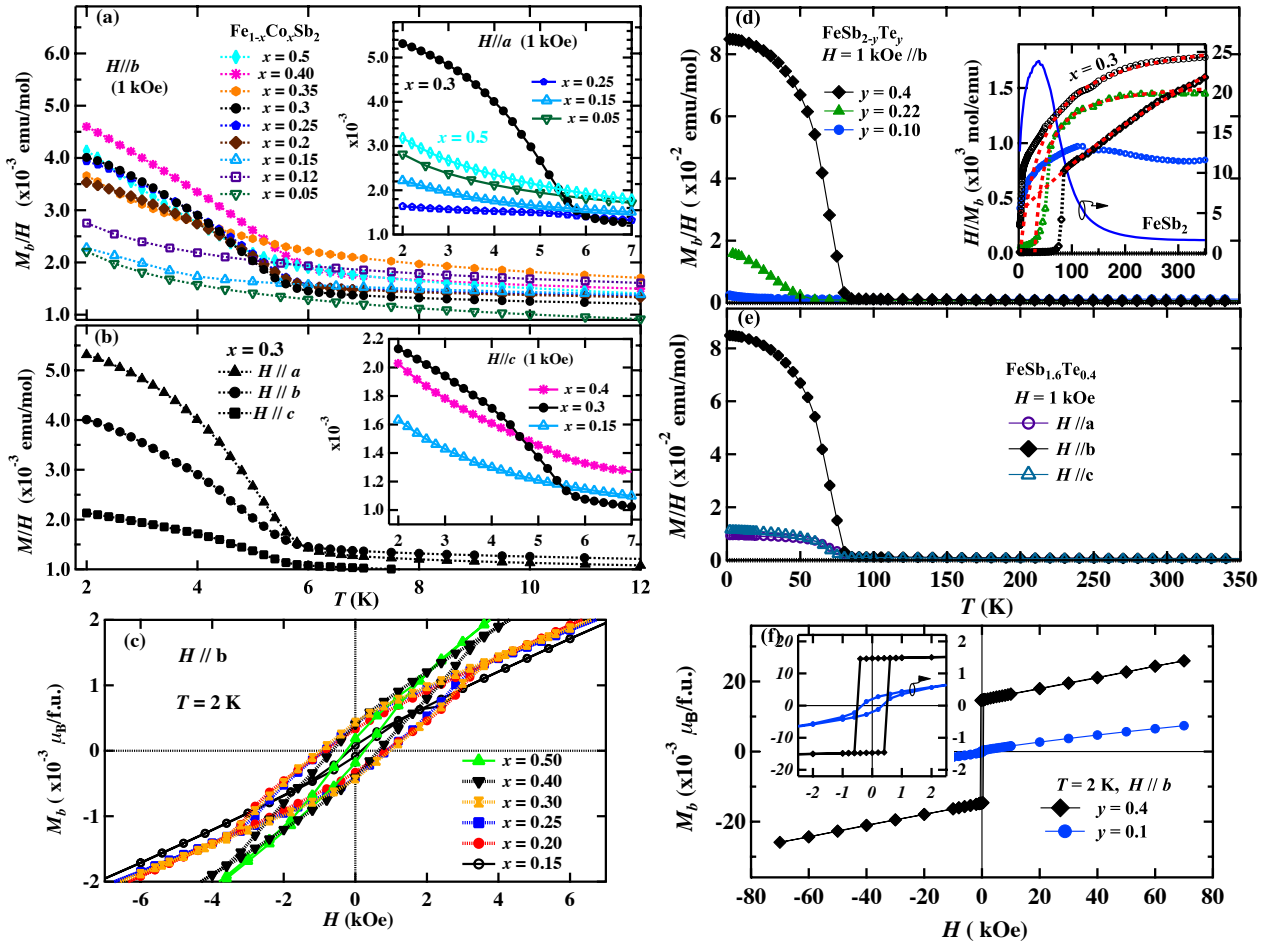


Figure 3: (a) Magnetic susceptibility $M(T)/H$ of $\text{Fe}_{1-x}\text{Co}_x\text{Sb}_2$ with x up to 0.5 under the field of 0.1 T applied along the b -axis. (b) Magnetic anisotropy of $\text{Fe}_{0.7}\text{Co}_{0.3}\text{Sb}_2$ under the field applied along the principal axes. Susceptibility data for different x doping under the fields applied along a and c axes are shown as insets in (a) and (b), respectively. (c) Magnetic hysteresis in the M - H curves of $\text{Fe}_{1-x}\text{Co}_x\text{Sb}_2$ with $H//b$. (d) $M(T)/H$ of $\text{FeSb}_{2-y}\text{Te}_y$ with y up to 0.4 under the field of 0.1 T applied along the b -axis. (e) Magnetic anisotropy of $\text{FeSb}_{1.6}\text{Te}_{0.4}$. (f) Magnetic hysteresis in the M - H curves of $\text{FeSb}_{2-y}\text{Te}_y$ with $H//b$. Inset of (d) shows the inverse susceptibility of $\text{FeSb}_{2-y}\text{Te}_y$ and $\text{Fe}_{0.7}\text{Co}_{0.3}\text{Sb}_2$. Dashed lines are the fits to a modified CW law.

decrease of the energy gap as well as the qualitative evolution of the emergent FM with Co ($3d$ electrons) and Te ($5p$ electrons) are identical, which imply the itinerant electron character of the magnetization that depends on the electron number in the conduction band rather than the magnetically active ions (Fe and Co). A nearly ferromagnetic semiconductor is the picture proposed for FeSb_2 as well as FeSi in the spin-fluctuation theory^{18,23}. The induced ferromagnetism in these strongly correlated low-carrier systems has been also discussed in the Kondo insulator scenario²⁴. Further, the concentration dependence of the magnetization per transition metal atom in $\text{Fe}_{1-x}\text{Co}_x\text{Sb}_2$, see table 1, agrees well with the observed concentration dependence in $\text{Fe}_{1-x}\text{Co}_x\text{Si}$ and accords with the prediction of a correlated band insulators model²⁵. However, the magnetically ordered state and the much higher Curie temperature and spontaneous moment by p -electron doping in $\text{FeSb}_{2-y}\text{Te}_y$ relative to those by d -electron doping in $\text{Fe}_{1-x}\text{Co}_x\text{Sb}_2$ system are yet to be further clarified.

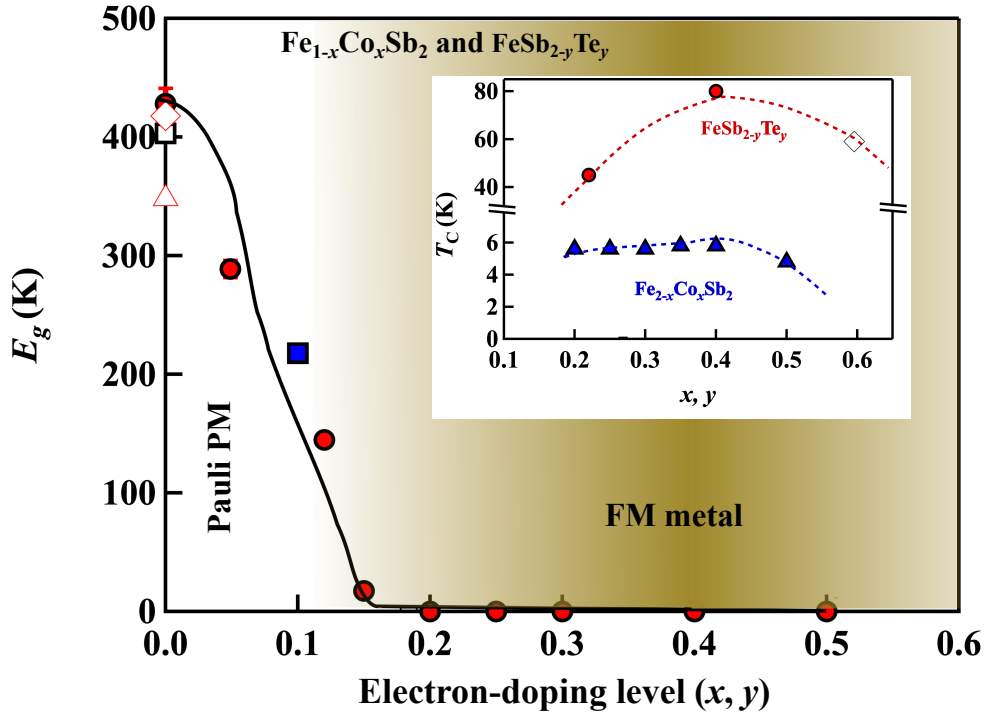


Figure 4: Magnetic phase diagram of $\text{Fe}_{1-x}\text{Co}_x\text{Sb}_2$ and $\text{FeSb}_{2-y}\text{Te}_y$, showing the evolution of the energy gap E_g , closed circles for $\text{Fe}_{1-x}\text{Co}_x\text{Sb}_2$ and closed square for $\text{FeSb}_{2-y}\text{Te}_y$ from magnetization data. Open diamond for FeSb_2 estimated from resistivity data in this work. Open square and triangle after Bentein et al. and Takahashi et al. respectively^{6,8}. The inset shows the composition dependence of T_C of $\text{Fe}_{1-x}\text{Co}_x\text{Sb}_2$ and $\text{FeSb}_{2-y}\text{Te}_y$, T_C for $y = 0.6$ (open diamond) is cited from reference²².

Table 1: Magnetic parameters of FeSb₂ and its electron-doped solid solutions.

x, y	χ_0 (10^{-4} emu/mol)	E_g (K)	T_C (K)	θ_W (± 3 K)	μ_{eff} ($\mu_B/\text{f.u.}$)	μ_s (10^{-4} $\mu_B/\text{f.u.}$)	μ_{eff}/μ_s
FeSb ₂							
0	0	428 (13)					
Fe _{1-x} Co _x Sb ₂							
0.05	4.39	289 (7)					
0.12	5.65	145 (3)					
0.15	5.45	17 (1)				0.8(2)	
0.2	6.56	0	5.6	5	0.386(11)	4.47(1)	863
0.25	7.04	0	5.6	16	0.408(57)	5.57(1)	732
0.3	4.95	0	5.6	3	0.411(1)	5.79(1)	710
0.35	1.96	0	5.8	3	0.623(3)	5.29(7)	1178
0.4	5.56	0	5.8	1	0.602(6)	4.94(1)	1219
0.5	2.95	0	4.8	4	0.536(4)	2.60(2)	2062
FeSb _{2-y} Te _y							
0.1	8.89	218 (5)				3.26(2)	
0.22	6.35	0	45	30	0.306(1)	17.07(1)	179
0.4	2.08	0	80	-70	1.180(1)	147.42(2)	80

4. Conclusion

We have successfully grown large single crystals of FeSb₂ and its electron-doped solid solutions, Fe_{1-x}Co_xSb₂ ($0 \leq x \leq 0.5$) and FeSb_{2-y}Te_y ($0 \leq y \leq 0.4$) with a simplified self-flux technique out of Sb flux. The high quality of grown single crystals has been indicated by XRD, WDX, Laue x-ray patterns, magnetization and resistivity results. The evolution from a Pauli paramagnetic state to itinerant-electron anisotropic ferromagnetic states with electron doping are observed. By employing the Takahashi's model of the itinerant-electron moment by thermal activation established in the spin fluctuation theory we have estimated the band gap, that consists with resistivity results, and its evolution with electron doping. We observed gradual decrease of the energy gap that closes with electron doping at about $x = y = 0.15$ followed by an emergent metallic ferromagnetic state. The magnetic phase diagram has been established and the results were briefly discussed in view of proposed scenarios with focus on the picture of nearly ferromagnetic narrow-gap semiconductor proposed in the spin fluctuation theory.

5. References

- ¹ Z. Xiang, Y. Kasahara, T. Asaba, B. Lawson, C. Insman, LuChen, K. Sugimoto, S. Kawaguchi, Y. Sato, G. Li, S. Yao, Y.L. Chen, F. Iga, J. Singleton, Y. Matsuda, and L. Li, *Science* **69**, 65 (2018).
- ² S. Wolgast, Ç. Kurdak, K. Sun, J.W. Allen, D.J. Kim, and Z. Fisk, *Phys. Rev. B* **88**, 180405 (2013).
- ³ Z. Schlesinger, Z. Fisk, H.T. Zhang, M.B. Maple, J. DiTusa, and G. Aeppli, *Phys. Rev. Lett.* **71**, 1748 (1993).
- ⁴ C. Petrovic, J.W. Kim, S.L. Bud'ko, a. I. Goldman, P.C. Canfield, W. Choe, and G.J. Miller, *Phys. Rev. B* **67**, 155205 (2003).
- ⁵ H. Tsunetsugu, M. Sigrist, and K. Ueda, *Rev. Mod. Phys.* **69**, 809 (1997).
- ⁶ A., S. Johnsen, G.K.H. Madsen, B.B. Iversen, and F. Steglich, *Europhys. Lett.* **80**, 17008 (2007).
- ⁷ H. Takahashi, R. Okazaki, S. Ishiwata, H. Taniguchi, A. Okutani, M. Hagiwara, and I. Terasaki, *Nat. Commun.* **7**, 12732 (2016).
- ⁸ P. Sun, N. Oeschler, S. Johnsen, B.B. Iversen, and F. Steglich, *Dalt. Trans.* **39**, 1012 (2010).
- ⁹ A. V. Lukoyanov, V. V. Mazurenko, V.I. Anisimov, M. Sigrist, and T.M. Rice, *Eur. Phys. J. B* **53**, 205 (2006).
- ¹⁰ M.A. Kassem, Y. Tabata, T. Waki, and H. Nakamura, *J. Phys. Conf. Ser.* **868**, (2017).
- ¹¹ H. Takahashi, Y. Yasui, I. Terasaki, and M. Sato, *J. Phys. Soc. Japan* **80**, 054708 (2011).
- ¹² V. Jaccarino, G.K. Wertheim, J.H. Wernick, L.R. Walker, and S. Arajs, *Phys. Rev.* **160**, 476 (1967).
- ¹³ T. Koyama, H. Nakamura, T. Kohara, and Y. Takahashi, *J. Phys. Soc. Japan* **79**, 093704 (2010).
- ¹⁴ Y. Takahashi, *J. Phys. Condens. Matter* **9**, 2593 (1997).
- ¹⁵ Y. Takahashi, *J. Phys. Condens. Matter* **10**, L671 (1998).
- ¹⁶ K. Koyama, T. Goto, T. Kanomata, and R. Note, *J. Phys. Soc. Japan* **68**, 1693 (1999).
- ¹⁷ H. Takahashi, R. Okazaki, I. Terasaki, and Y. Yasui, *Phys. Rev. B* **88**, 165205 (2013).
- ¹⁸ T. Deguchi, K. Matsubayashi, Y. Uwatoko, T. Koyama, T. Kohara, H. Nakamura, Y. Mitsui, and K. Koyama, *Mater. Trans. advpub*, (2020).
- ¹⁹ M. Imada, A. Fujimori, and Y. Tokura, *Rev. Mod. Phys.* **70**, 1039 (1998).
- ²⁰ R. Hu, V.F. Mitrović, and C. Petrovic, *Phys. Rev. B* **74**, 195130 (2006).
- ²¹ R. Hu, V.F. Mitrović, and C. Petrovic, *Phys. Rev. B* **76**, 1 (2007).
- ²² R. Hu, V.F. Mitrović, and C. Petrovic, *Phys. Rev. B* **79**, 064510 (2009).
- ²³ K. Koyama, T. Goto, T. Kanomata, R. Note, and Y. Takahashi, *J. Phys. Soc. Japan* **69**, 219 (2000).
- ²⁴ S. Yeo, S. Nakatsuji, A.D. Bianchi, P. Schlottmann, Z. Fisk, L. Balicas, P.A. Stampe, and R.J. Kennedy, *Phys. Rev. Lett.* **91**, 046401 (2003).
- ²⁵ V. V. Mazurenko, A.O. Shorikov, A. V. Lukoyanov, K. Kharlov, E. Gorelov, A.I. Lichtenstein, and V.I. Anisimov, *Phys. Rev. B* **81**, 125131 (2010).